 doi:10.20944/preprints201611.0083.v4

A Semi-empirical Model of Air Waves Induced by Falling Rock in a Closed Goaf

Fengyu Ren[1], Yang Liu [1*], Jianli Cao[1], Rongxing He[1], Yuan Xu[1], Xi You [1], Yanjun Zhou[1]

[1] School of Resources and Civil Engineering, Northeastern University, Shenyang, Liaoning Province, China

[*]Correspondence: liuyang1510448@gmail.com; Tel.: +86-24-83678401

Abstract: In this paper, a semi-empirical model of air waves induced by falling rock is described. The model is composed of a uniform motion phase (velocity close to 0 $m \cdot s^{-1}$) and an acceleration movement phase. The uniform motion phase was determined based on experimentally and the acceleration movement phase was derived by theoretical analysis. A series of experiments were performed to verify the semi-empirical model and elucidated the law of the uniform motion phase. The acceleration movement phase accounted for a larger portion with a greater height of the falling rock. Experimental results of different falling heights of the goaf showed close agreement with theoretical analysis values. The semi-empirical model could accurately and conveniently estimate the velocity of air wave induced by falling rock. Thus, the semi-empirical model can provide a reference and basis for estimating the speed of air waves and designing protective measures in mines.

Keywords: air waves; falling rock; semi-empirical model; uniform motion phase; acceleration movement phase

 doi:10.20944/preprints201611.0083.v4

1. Introduction

In recent years, failures involving falling rock and the collapse of surfaces has occurred more frequently, which has created a serious risk of injury and damage to people and mines [1-3]. In these mine disasters, the resulting air wave typically has high velocity, high pressure, a massive impact force and a short effective duration [4]. To accurately measure the size and impact of this type of disaster, various models have been built to predict the velocity of the air wave [5-6]. Chen et al. [5] modeled the shock process as a compression process, which has a higher velocity than in the real-life conditions. Zheng et al. [6] proposed that the shock process be combined with the compression and airflow process, but the formulation of the model was not described. To estimate the velocity of air waves induced by falling rock more accurately and conveniently, the semi-empirical model is used in the present. Then according to the prediction of air waves' velocity, protective measures were designed to reduce the damage.

Experimental research—the most common method—can not only obtain the true value of the air waves' velocity, but also analyze the influence of the height of the falling rocks. To that end, Janovsky et al. [7] used methane and air as the tested materials to analyze the velocity and the impact on walls whose thicknesses were 14 and 29 cm thick. Mixed air has also been adopted in many experiments [8-10]. Xing et al. [11] revealed complex influences of goaf from different cave in areas on the velocity and pressure of the air shock waves in different mining faces. Pennetier et al. [12] performed air shock experiments in a tunnel and presented the evolution of the pressures and velocities of both the inlet and outlet tunnel in detail with the measurements on different blast volumes. However, the test instruments used in previous experiments were not the same, and have included a thermal anemometer

Preprints (www.preprints.org) | NOT PEER-REVIEWED | Posted: 25 January 2017 doi:10.20944/preprints201611.0083.v4

[13], differential-pressure anemometer[14], and ultrasonic anemometer[15]. Ovink et al. [16] used a hot wire hot film anemometer as a test instrument. The results acting conform to the actual values during travel over experimental material.

In this paper, we present a semi-empirical model for air waves induced by falling rock in a closed goaf to efficiently predict the velocity of the air wave. Specifically, the model is composed of a uniform motion phase and an acceleration movement phase. The uniform motion phase was determined by experience, and the acceleration movement phase was derived using a theoretical analysis. Then, a series of experiments were conducted to verify the semi-empirical model and elucidated the law of the uniform motion phase. Finally, we evaluated the effectiveness of our model and compared its performance with experimental values. The results showed that the semi-empirical model could estimate the velocity of air wave induced by falling rock accurately and easily. Furthermore, the semi-empirical model could provide a reference and basis for estimating the velocity of air waves and designing protective measures in mines.

2. Modeling Description of the Acceleration Movement Phase

2.1 Basic Assumptions

Based on the model of pump [5] and streaming [6], a semi-empirical model was built to estimate the air waves induced by falling rock. The model was composed of the uniform motion phase and the acceleration movement phase. The speed of the uniform motion phase was nearly 0 $m \cdot s^{-1}$ due to the pressure difference. The acceleration movement phase was derived from both computational fluid mechanics

Preprints (www.preprints.org) | NOT PEER-REVIEWED | Posted: 25 January 2017 doi:10.20944/preprints201611.0083.v4

and classical mechanics. Then, the assumptions of the acceleration movement phase were as follows:

(a) Air was considered an ideal gas and characterized by laminar flow conditions;

(b) The process of the air wave was identified as an isothermal process;

(c) The goaf was considered closed, and the volume difference of the goaf was neglected;

(d) The pressure of the outlet tunnel was regarded as standard atmospheric pressure.

2.2 Modeling Equations

The governing equations used in our 2D, isothermal model are described below. The law of conservation of momentum [17,18] is shown as follows:

$$\rho \frac{dv}{dt} = \rho F_i - \frac{\partial p}{\partial x_i} + \mu \Delta v \qquad (1)$$

Where Δ is the Laplace operator; ρ is the density of air in the goaf, $(Kg \cdot m^{-3})$;F_i is the body force, (N); μ is the viscosity of air, $(Pa \cdot s)$; v is the air velocity, $(m \cdot s^{-1})$.

According to the above assumptions, the value for μ is 0 and the value for ρ is obtained from the ideal law, $\rho = p / RT$, in which R is the universal gas constant and T is the absolute temperature. The weight of falling roof act as the body force. Eq. (1) is simplified as follows:

$$\frac{\partial v_z}{\partial t} = g - \frac{p_n - p_{n-1}}{\rho_d N} \qquad (2)$$

Where ρ_d is the density of the falling rock, $(kg \cdot m^{-3})$; N is thickness of the falling rock, (m); P_n and P_{n-1} are the pressure of adjacent time periods in the falling process, (Pa); v_z is the vertical velocity of air in the goaf, $(m \cdot s^{-1})$; g is the gravitational acceleration, $(m \cdot s^{-2})$.

In our model, the ideal gas state equation [38] is described as follows:

$$p_n V_n = p_{n-1} V_{n-1} \qquad (3)$$

Where Vn and V_{n-1} are the falling volume of adjacent time periods during the falling process, (m^3).

Preprints (www.preprints.org) | NOT PEER-REVIEWED | Posted: 25 January 2017 doi:10.20944/preprints201611.0083.v4

Due to the condition of the model, the initial falling height of the acceleration movement phase was not 0 *m*, but rather the final height of the uniform motion phase. As a result, V_n is obtained from the equation, $V_n = (H - H_m - H_n) \cdot S$, where H is the height of goaf, (*m*); H_m is the final height of the uniform motion phase, (*m*); H_n is the falling height of the acceleration movement phase, (*m*); S is the area of the goaf, (m^2).

The volume can be calculated from the following equation:

$$p_n = \frac{H - H_m - H_{n-1}}{H - H_m - H_n} \cdot p_{n-1} \tag{4}$$

Where H_n and H_{n-1} are the falling height of adjacent time periods in the acceleration movement phase, (*m*).

On the basis of Newton's Law, the velocity and the falling height can be obtained:

$$H_n = H_{n-1} + v_{n-1} \cdot \Delta t \tag{5}$$

$$v_n = v_{n-1} + \left[g - \frac{(H_n - H_{n-1}) \cdot p_{n-1}}{\rho_d N (H - H_m - H_n)} \right] \cdot \Delta t \tag{6}$$

Where v_n and v_{n-1} are is the air speed of adjacent time periods in the goaf, ($m \cdot s^{-1}$) ; Δt is the time step, (*s*).

The acceleration movement phase controlled by Eqs. (4), (5) and (6) is multiphysical in nature. The three unknowns (*P, v, H*) to be solved depend on one another, as shown in Eq. (6). The dynamics of these unknowns are different from each other in the sense that typically, compared to pressure, speed and height vary on a time scale. The implicit pressure explicit saturation(IMPES) scheme [19] was proposed to solve this problem. In addition, the operator decomposition technique with which the unknowns (*P,H)* are decoupled from the velocity *v* by lagging one time step behind calculations was used. This approach enabled P_n and H_n to be solved

Preprints (www.preprints.org) | NOT PEER-REVIEWED | Posted: 25 January 2017 doi:10.20944/preprints201611.0083.v4

implicitly, giving v_{n-1}. Next, (P_n, H_n) was used to solve v_n explicitly. The IMPES scheme is listed in Fig 1. [20].

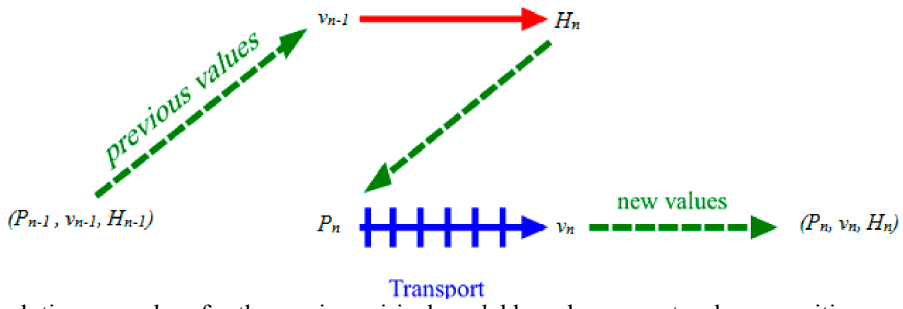

Figure 1. A solution procedure for the semi-empirical model based on operator decomposition

Because the outlet was linked with the goaf, the air wave in the outlet was applied to the Bernoulli equation [21]; the air waves' velocity in the outlet can then be calculated from the following equation:

$$v_b = \sqrt{\frac{2(p_{bn} - p_{b0}) + v_n^2 \rho_n}{9.8 + \rho_L}} \tag{7}$$

Where v_b is the velocity of the outlet, $(m \cdot s^{-1})$; p_{bn} is the pressure of the outlet, (Pa); p_{bo} is the initial pressure of the outlet, (Pa); ρ_n is the density of air in the goaf, $(kg \cdot m^{-3})$; ρ_L is the density of air in the outlet, $(kg \cdot m^{-3})$. As a result of the above assumption (d), P_{b0} is the standard atmospheric pressure.

According to the on-site experiment, the area of the falling roof was smaller than the area of the goaf. Based on the air quantity balancing law, the pressure of the outlet can be obtained as follows:

$$p_{bn} = \frac{S_b}{S - S_a + S_b} p_n \tag{8}$$

Where S is the sectional area of the goaf, (m^2); S_a is the sectional area of the falling roof, (m^2); S_b is the sectional area of the outlet, (m^2).

Substituting Eq. (8) into Eq. (7), the following was obtained:

Preprints (www.preprints.org) | NOT PEER-REVIEWED | Posted: 25 January 2017 doi:10.20944/preprints201611.0083.v4

$$v_b = \sqrt{\frac{2S_b(p_n - p_0) + v_n^2 \rho_n}{(9.8 + \rho_L)(S - S_a + S_b)}} \tag{9}$$

Where P_0 is the initial pressure of the goaf, (Pa).

3. Experiment

3.1 Experimental Setup

An experimental setup was built to investigate the air wave induced by falling rock in the closed goaf, as shown in Fig 2. The experimental setup consists of the air wave generator (Fig 3.), the hot wire hot film anemometer (HWFA) of IFA300 (Fig 4.), a data collection system and other components.

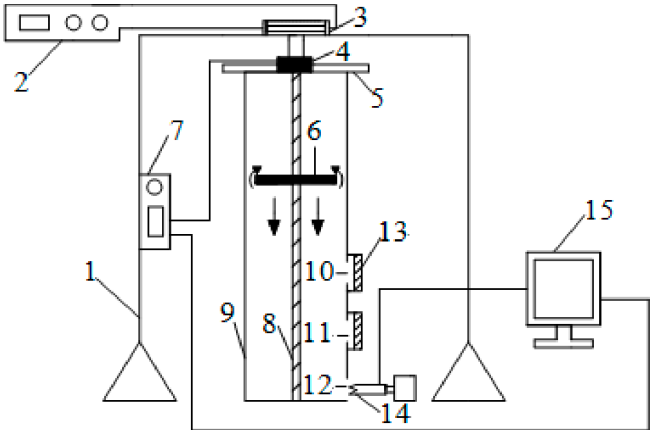

Figure 2. Experimental setup.

(1- the rigid frame, 2- alternating current power supply, 3- the hoist, 4-electromagnetic relays, 5-capping, 6- iron salver, 7- control switch, 8- fixed link, 9- the tank, 10- #3 outlet tunnel, 11- #2 outlet tunnel, 12- #1 outlet tunnel, 13- valve, 14- the probe of HWFA of IFA300, 15- the data collection computer).

Preprints (www.preprints.org) | NOT PEER-REVIEWED | Posted: 25 January 2017 doi:10.20944/preprints201611.0083.v4

Figure 3. The air wave generator.

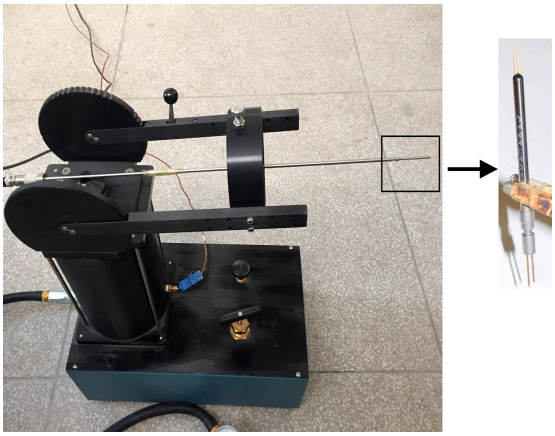

Figure 4. The hot wire hot film Anemometer of IFA300.

The air wave generator was composed of a tank, outlet, hoist and iron salver. The tank, with a diameter of 0.1 *m* and height of 1.25 *m*, was cylinder-shaped and fixed on the ground. The #1 outlet was installed 0.05 *m* above the bottom of the tank with the square of 0.03 *m*, and the #2-3 outlets were set up on the upper side. The #2 outlet was 0.35 *m* away from the bottom of the tank, and the #3 outlet was 0.6 *m* away from the top of the tank. The outlet tunnel was linked to the outlet with a length of 0.1 *m*. The upper side of the tank was closed. The probe of HWFA of IFA300 was placed in the tunnel outlet. The iron salver was circular with a 0.09 *m* diameter and thickness of 0.01 *m*, and a density of 4500 $Kg \cdot m^{-3}$. To verify the effectiveness of the semi-empirical model, the experiments were performed using three groups with different falling heights of 0.6 *m*, 0.9 *m* and 1.2 *m*. After running the experiment 3 times for each group, we calculated the averages as the experimental data points

3.2 Experimental Results and Discussion

The velocities of the air waves after releasing the iron salver from the different falling heights are shown in Fig 5. As shown in Fig 5., the three curves followed the same trend, the velocity curves were composed of a straight line and a rapid growth curve. In addition, the semi-empirical model was possible to estimate the air waves' velocity.

Preprints (www.preprints.org) | NOT PEER-REVIEWED | Posted: 25 January 2017 doi:10.20944/preprints201611.0083.v4

At the phase of uniform motion, as the tank was closed, a huge pressure difference would be engendered in the tank with as the iron salver descended, preventing the air wave from reaching the outlet. At the phase of the straight line, reducing the boundary of pressure difference was a major factor in the rapid growth of velocity. Therefore, the realistic air wave was composed of the phase of acceleration movement and uniform motion.

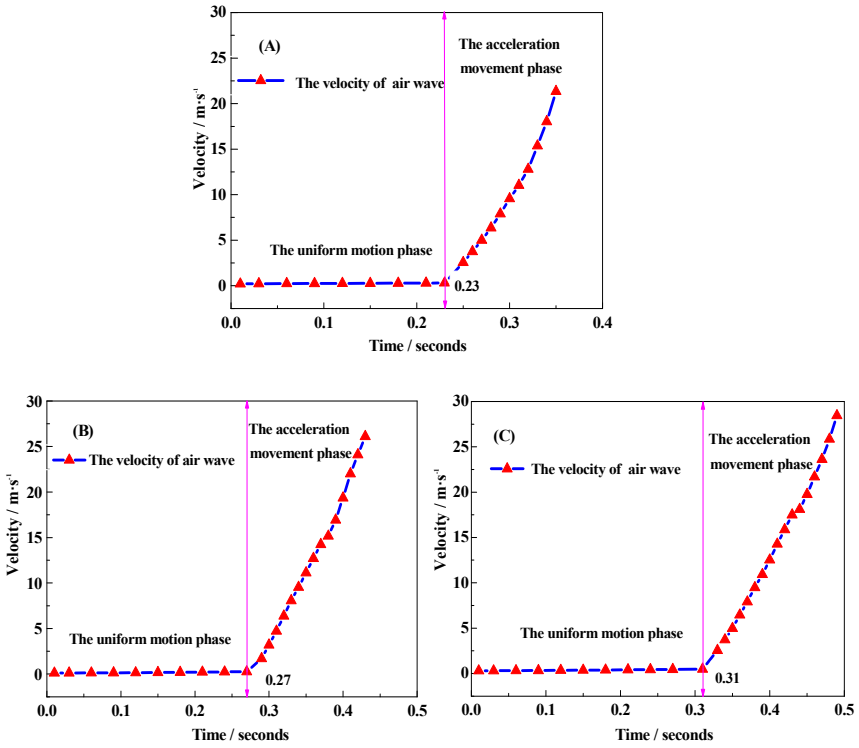

Fig 5. Relationship between velocity and time with different falling heights. (A) 0.6 *m*. (B) 0.9 *m*. (C) 1.2 *m*.

According to the experimental results, a large pressure difference was generated by the descent of the iron salver. The air was regarded as incompressible due to the process of the experiment being transient. The upper part of the iron salver raised the zone of negative pressure and the bottom presented positive pressure, while the outlet maintained a normal pressure [22]. The air on the bottom would burst towards the upper side and outlet. If the pressure difference between the upper and bottom parts could absorb enough air, a siphon phenomenon would form on lower side, causing the

Preprints (www.preprints.org) | NOT PEER-REVIEWED | Posted: 25 January 2017 doi:10.20944/preprints201611.0083.v4

stage of uniform motion to commence. Otherwise, the stage of acceleration movement would commence.

Fig 5. shows that the velocity of 0.9 m and 1.2 m heights showed the same trend as that of the 0.6 m height, although that the phase of uniform motion was more obvious and the peak value was much higher at the former two heights .The velocity of the 1.2 *m* release height was largest, followed by the 0.9 *m* and 0.6 *m* heights, with the values of 21.3488 $m{\cdot}s^{-1}$, 26.1003 $m{\cdot}s^{-1}$ and 28.4508 $m{\cdot}s^{-1}$ respectively, and the time phases of uniform motion were 0.23 *s*, 0.27 *s* and 0.31 *s* respectively. The turning points of the uniform motion phase and acceleration movement phase were located at 0.2645 *m*, 0.3645 *m*, 0.4805 *m* in the above release heights. According to Eq. (6), the pressure difference was inversely proportional to the falling height. As a result, the phase of the acceleration movement became extended. This result indicates that the phase of acceleration movement took longer and the uniform motion was shorter when the height of the falling rock was higher. However, increasing the height of the falling rock strengthen the function of time in the pressure difference. Hence, when the falling roof was higher, the growth rate of the acceleration movements' phase was slower. Because it occupied a larger portion, when the falling roof was higher, the air waves' velocity would also be higher. However, the peak values of velocity were not in direct proportion to the release heights. The closed goaf can reduce the damage of air waves but not completely eliminate it.

3.2.1 The Uniform Motion Phase

Fig 5. shows that there was a linear relation between the height of the uniform motion phase and the falling height of rock. The relation between these variables can be expressed as follows:

$$H_m = aH + b \tag{10}$$

Preprints (www.preprints.org) | NOT PEER-REVIEWED | Posted: 25 January 2017 doi:10.20944/preprints201611.0083.v4

Where H_m corresponds to the height of the uniform motion phase, (m); a and b are the parameters of the curve; and H is the falling height, (m). The values for a and b for the uniform motion phase are 0.36 and 0.04583 m respectively, with a coefficient of determination R^2 equal to 0.99635.

3.2.2 The Acceleration Movement Phase

According to the experimental setup and Eq. (10), the parameters for both conditions, the different falling heights are summarized in Table 1.

Table 1. The parameters for acceleration movement phase

H (m)	S_a (m^2)	S_b (m^2)	ρ_d ($Kg\times m^{-3}$)	N (m)	p_0 (Pa)	ρ_0 ($Kg\times m^{-3}$)	g ($m\times s^{-2}$)	t (s)	H_m (m)
0.6	0.00636	0.0009	4500	0.01	103360	1.225	9.8	0.12	0.2645
0.9	0.00636	0.0009	4500	0.01	103360	1.225	9.8	0.16	0.3645
1.2	0.00636	0.0009	4500	0.01	103360	1.225	9.8	0.18	0.4805

Eq. (1) to Eq. (9) were solved using the above coefficients. The experimental values and theoretical values of the air waves' velocity in the acceleration movement phase is shown in Fig 6. As shown in Fig 6., the experimental values and theoretical values followed the same trend.

The relative errors between experimental results and theoretical analysis of the acceleration movement phase could then be calculated from the following equation:

$$\delta = \frac{|v_{1n} - v_{2n}|}{v_{1n}} \times 100\% \qquad (11)$$

Where δ is the relative error,($\%$); v_{1n} is the experimental value, ($m\cdot s^{-1}$); v_{2n} is the theoretical value, ($m\cdot s^{-1}$).

The relative errors are shown in Fig 7. for different falling heights. The relative errors were almost 10% lower, and the relative errors of cut-off velocity were 1.87%, 0.50% and 3.26% respectively. Because the probe of HWFA of IFA300 was placed in the tunnel outlet, the air movements in the laboratory affected on the experimental results. In addition, the initial points of the acceleration movement phase were too

Preprints (www.preprints.org) | NOT PEER-REVIEWED | Posted: 25 January 2017 doi:10.20944/preprints201611.0083.v4

small and thus led to a large error in the relative errors. However, when the air waves' velocity was higher, the impact of external wind was lower. As a result, the prediction precision of the semi-empirical model increased.

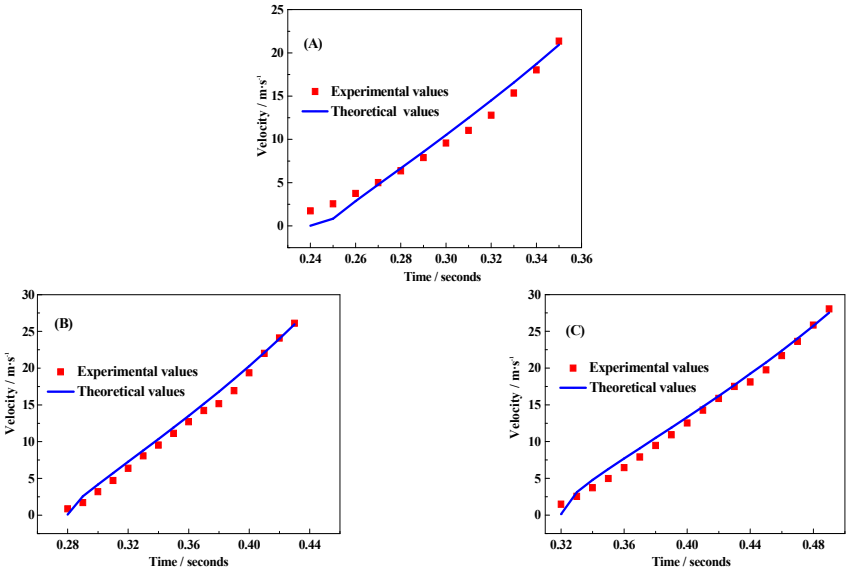

Figure 6. Velocity estimation using Eq. (10) versus experimental values with the different falling heights.

(A) 0.6 *m*. (B) 0.9 *m*. (C) 1.2 *m*.

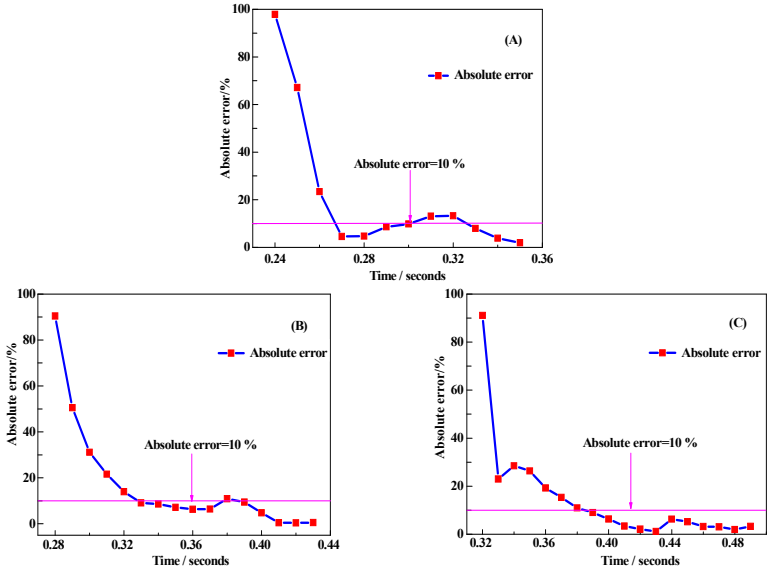

Figure 7. The relative error between experimental results and theoretical analysis with different falling heights

(A) 0.6 *m*. (B) 0.9 *m*. (C) 1.2 *m*.

Preprints (www.preprints.org) | NOT PEER-REVIEWED | Posted: 25 January 2017 doi:10.20944/preprints201611.0083.v4

These results show good agreement between experimental values and theoretical results. This correlation demonstrates that despite the small differences due to experimental error, the semi-empirical model provides an accurate evaluation nethod.

The calculation formula of the semi-empirical model follows:

$$v_b = \begin{cases} 0 & H_m \le 0.36H + 0.04583 \\ \sqrt{\dfrac{2S_b(p_n - p_0) + v_n^2 \rho_n}{(g + \rho_L)(S - S_a + S_b)}} & H_m > 0.36H + 0.04583 \end{cases} \quad (12)$$

4. Conclusions

In this paper, we proposed and verified a semi-empirical model of air waves' velocity induced by falling rock using theoretical analysis and experiments. We developed a semi-empirical model composed of a uniform motion phase(velocity close to 0 $m{\cdot}s^{-1}$) and an acceleration movement phase through theoretical analysis. Satisfactory agreement was observed between the model and experimental results with respect to the values surveyed in the field for the velocity and the variation trend of the air wave demonstrating the effectiveness of the model. A comparison between the experimental results using the groups with different falling roof heights showed that the acceleration movement phase was of a longer duration and the uniform motion phase was shorter when the falling roof was higher. The calculation formula of the semi-empirical model was obtained.

This paper proposed a semi-empirical model to estimate the air waves' velocity induced by falling rock in a closed goaf, providing a method with which to estimate the air waves' velocity and design protective measures in mines. The semi-empirical model could estimate the velocity of air waves induced by falling rock accurately and easily. In addition, the semi-empirical model could provide a reference and basis for estimating the air waves' velocity and designing protective measures.

Acknowledgments: This research was supported by the National Natural Science Foundation of China(No. 51534003, 51404065), the National "Thirteenth Five-Year" Plan for Science and Technology Support(No. 2016YFC0801601), and the Fundamental Research Funds for the Central Universities(No. N140104008, N150104006).

Conflicts of Interest: The authors declare no conflict of interest.

References

1. Gao, F.; Wu, Y.; Stead, D.; Kang, H. Discrete element modelling of deformation and damage of a roadway driven along an unstable goaf — A case study. International Journal of Coal Geology. 2014, 127(7), 100-110.

2. Hao, T.X.; Jin, Z.C.; Li, F. Optimization of goaf gas drainage parameters based on numerical simulation studying fracture in overlying strata. Procedia Engineering. 2012, 43(9), 337-338.

3. Wang, G.; Cheng, W.; Xie, J. Field Test Research on Two-dimensional Gas Concentration and Temperature Distribution in the Goaf of Fully Mechanized Caving Face. Procedia Engineering. 2012, 43(43), 478-483.

4. Dong, B.C. Study on The Prevention and Prediction of Surrounding Rock Caving Hazard in The 2# Goaf Dongshenmiao Mine[Dissertations]. Baotou: Inner Mongolia University of Science and Technology; 2015. Chinese.

5. Chen, Q.K.; Ren, F.Y. Li, Q.W.; Tao, G.Q. [Study on the Technical Measures for Controlling the Roof-fall in Mined Area]. Metal Mine. 2002,316(10), 7-9. Chinese.

6. Zheng, H.C.; Song, C.Y.; Hu, L.; Xiao, G.; Li, M.; Zhang, X.J. [Simulation of air shock waves induced by large-scale roof caving in huge mined-out area](in). Journal of University of Science & Technology Beijing. 2010, 32(3), 277-281. Chinese.

7. Janovsky, B.; Selesovsky, P.; Horkel, J.; Vejsa, L. Vented confined explosions in Stramberk experimental mine and AutoReaGas simulation. Journal of Loss Prevention in the Process Industries. 2006, 19(2–3), 280-287.

8. Rigas, F.; Sklavounos, S. Experimentally validated 3-D simulation of shock waves generated by dense explosives in confined complex geometries. Journal of Hazardous Materials. 2005, 121(1-3), 23-30.

9. Latter, R.; Similarity Solution for a Spherical Shock Wave. Journal of Applied Physics. 1955, 26(8), 954-960.

10. Jones, D.L. Strong Blast Waves in Spherical, Cylindrical, and Plane Shocks. 1961, 4(2), 1183-1184.

11. Xing, P.W.; Fu, Y.P.; Li, Z.J.; Song, X.M. [Coupling Model of Stope Roof with Hurricane Disaster and the Influence Analysis of Mining Height on Hurricane Velocity]. Journal of North University of China. 2010, 31(3), 228-231. Chinese.

12. Pennetier, O.; William-Louis, M.; Langlet, A. Numerical and reduced-scale experimental investigation of blast wave shape in underground transportation infrastructure. Process Safety & Environmental Protection. 2015, 94, 96-104.

13. Sazhin, O. Liquid Flow Meter based on a Thermal Anemometer Microsensor. Journal of Applied Fluid Mechanics. 2016, 9(4), 1991-1996.

14. Khimji, H. inventor. Differential pressure anemometer: United States patent, US 8342036 B2[P]. 2013.

15. Grandpeix, J.Y.; Lafore, J.P. A Density Current Parameterization Coupled with Emanuel's Convection Scheme. Part I: The Models. Journal of the Atmospheric Sciences, 2016, 67(4), 881-897.

16. Ovink, R.; Lamers, A.P.G.G.; Steenhoven, A.A.; Hoeijmakers, H.W.M. A method of correction for the binormal velocity fluctuation using the look-up inversion method

for hot-wire anemometry. Measurement Science & Technology. 2001, 12(8), 1208-1213.

17. Travis, J.R.; Koch, D.P.; Xiao, J.; Xu, Z. Real-gas Equations-of-State for the GASFLOW CFD code. International Journal of Hydrogen Energy. 2013 ,38(19), 8132-8140.

18. Hurly, J.J.; Schmidt, J.W.; Gillis, K.A. Virial equation of state and ideal-gas heat capacities of pentafluoro-dimethyl ether. International Journal of Thermophysics. 1997, 18(1), 137-159.

19. Aziz, K.; Settari, A. Petroleum Reservoir Simulation. Applied Science Publishers, Barking ;1979.

20. Ginting, V.; Lin, G.; Liu, J. On Application of the Weak Galerkin Finite Element Method to a Two-Phase Model for Subsurface Flow. Journal of Scientific Computing, 2016, 66(1),1-15.

21. Swan C. BERNOULLI EQUATION[J]. A-to-Z Guide to Thermodynamics Heat and Mass Transfer and Fluids Engineering, 2006, b.

22. Langefors, U.; Kihlström, B. The modern technique of rock blasting. Weinheim: Wiley; 1963.